*Texture of Crystalline Solids*
1979, Vol. 3, pp. 149-168



# PLASTIC DEFORMATION AND CRYSTALLINE TEXTURE IN EQUIBIAXIAL EXPANSION

C. GASPARD, P. MESSIEN, J. MIGNON AND T. GREDAY
*Center for Research in Metallurgy (C.R.M.), Liège, Belgium*

*(Received December 14, 1978)*

*Abstract:* The classical three-dimensional analysis (O.D.F.) has been extended in such a manner as to obtain the representation of the texture, and, more precisely, the distribution of the slip systems <111>{hkℓ} in the planes where shear stresses induced in equibiaxial expansion are maximum.

Quantification of the slip systems configuration allows the development of a deformation model which takes into account the factors influencing the degree of stretchability of the steels. From this model it is possible to define true hardening rates and equibiaxiality coefficients characterizing the ability of the steel to distribute the deformation in the macroscopic shear planes.

In association with the resistance to thinning defined by the configuration of the slip systems, the theoretical treatment makes it possible to grade different steels according to their experimental behavior.

## 1. INTRODUCTION

A mathematical model for calculation of plastic deformations with the objective of predicting the distributions of local deformations in drawn pieces has been formulated at our laboratory.[1]

In its simple version, this model regards plastic deformation as resulting from the superposition of plastic flows in maximum shear planes located at 45° from the axes of principal stresses, and is, therefore, not valid for anisotropic (textured) materials.

The complete calculation of plastic behavior will therefore require a preliminary examination of the slip systems that are really active; and this will make it necessary to

take their orientations into account in the calculation of the deformations.

The crystalline texture of steel sheets for drawing applications can most precisely be represented by the three-dimensional orientation distribution function.[2-4] Even with this texture representation, it is difficult to visualize the various slip systems capable of being activated during deformation.

For this reason we have extended the classical three-dimensional analysis (O.D.F.) in such a manner as to obtain the representation of the texture, and, more precisely, the distribution of the slip systems <111>{hkℓ} in the planes where shear stresses are maximum.[5] Our analysis is concerned particularly with biaxial expansion.

In the first stage, we describe the textures of three steels and their modifications during biaxial expansion. The crystalline orientations are then described in the planes at 45° from the principal axes, and this enables us to reveal the slip systems <111>{hkℓ} in these planes.

By geometrical considerations it is then possible to quantify the density of the slip systems in these maximum shear planes. This quantification constitutes a starting point for the introduction of the crystalline texture into the stress-strain relationships during biaxial deformation.

## 2. ANALYSIS OF DEFORMATION TEXTURES

### 2.1. Stretchability of the Steels

Texture analysis was made for three mild steels (Table I) of which the stretchability is different as is shown

TABLE I

CHARACTERIZATION OF STEELS

| Reference | Steels | $\bar{r}$ | $\bar{n}$ | n* | $\bar{d}(\mu)$ |
|---|---|---|---|---|---|
| A | Decarb.-denitr. | 1.74 | 0.188 | 0.309 | 26 |
| B | H.S.L.A. | 1.20 | 0.155 | 0.177 | 7 |
| C | Stabilized L.D. | 1.57 | 0.195 | 0.199 | 12 |

by comparing the variations of polar deformations in thickness as a function of polar height during bulge testing of these steels (Fig. 1). The results show that it is possible to classify the steels in the order B, A, C, with the steel C having the best stretchability. This classification cannot be explained on the basis of the classical mechanical characteristics of the steels and more particularly the $\bar{r}$ and $\bar{n}$-values (Table I).

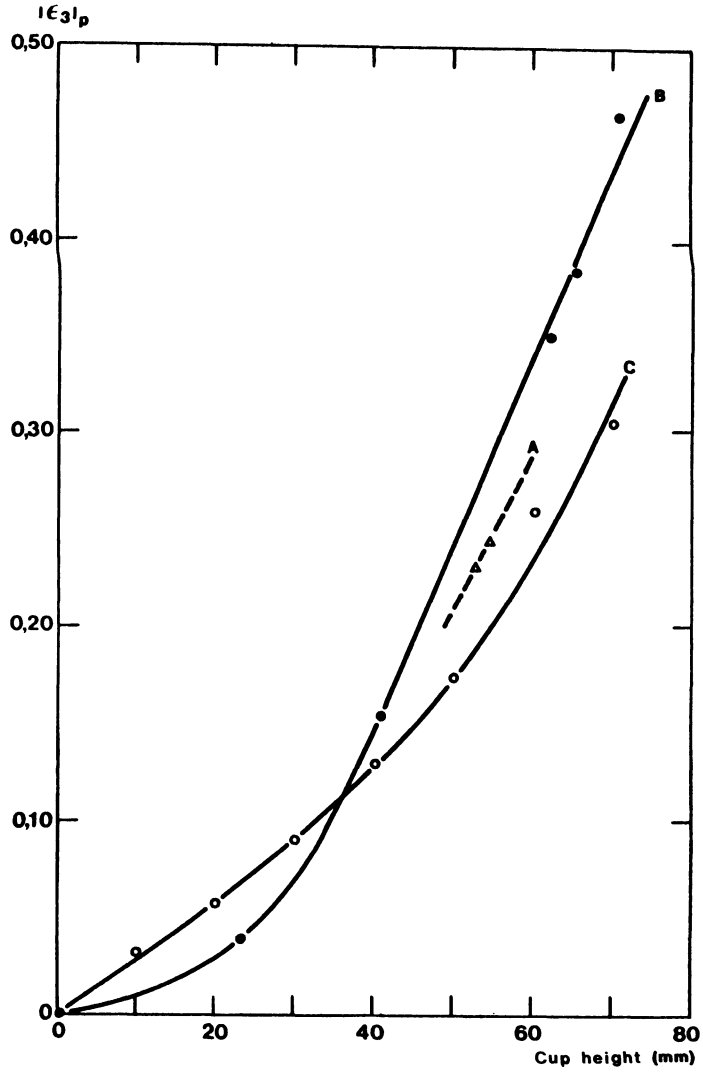


Fig. 1. Polar strain $|\varepsilon_3|_p$ as a function of the cup height (bulge test).

The measurements of principal strains $\varepsilon_1$, $\varepsilon_2$ by means of a millimetric grid (circles of 2 mm) previously set on the sheet, and the calculation of the corresponding principal stresses, $\sigma_1$, $\sigma_2$ on the basis of measurements of pressure, of thicknesses and of radii of curvature of the sheet allow the determination of the principal stress-strain relationships and of the strain hardening rate coefficients n* during bi-axial expansion[1,2] (Table I). These coefficients n* do not seem to correlate with the behavior of the steels and their classification (Fig. 1).

Biaxial expansion thus appears as a complex process which cannot be interpreted only by the characteristics of the

plastic anisotropy and strain hardening rate coefficients. The former appears as an excessively rough approximation to the original crystalline texture and takes its modifications during expansion into account only to a very small extent; whereas the latter is a parameter too complex to distinguish the true behavior of the material from the interferences due to the rotations of the crystals (modifications of texture), particularly at high strains.

### 2.2. Crystalline Textures Analysis

The crystalline textures were determined not only before deformation ($\varepsilon = 0$) but also at different states of deformation by equibiaxial expansion, in order to characterize the texture modifications of the three steels during deformation. Samples for texture analysis were machined from the top of cups drawn at different pressures; these samples were sufficiently small to allow the deformation in thickness to be regarded as constant. The following drawing parameters characterize each sample: deformation in thickness $|\varepsilon_3|_p$, main stresses $\sigma_1 \equiv \sigma_2$ along the rolling (RD) and transverse (TD) directions (Table II).

The three-dimensional representation of the texture called in each case for the determination (Siemens-Lücke goniometer) of the two complete pole figures {200} and {211} and the calculation of the orientations distribution functions.[4] This three-dimensional representation reveals many differences regarding not only the non-deformed states but also the development of texture components during expansion.

### 2.3. Textures Before Deformation

In the three cases, the textures are characteristic of mild steels for drawing and thus have strong components of the partial fiber texture <111>//ND (Figs. 2 to 4). The strength of these components is not directly related to the plastic anisotropy coefficient $\bar{r}$. The relative strength of the textures $(\bar{1}11)[1\bar{1}2]$ and $(\bar{1}11)[0\bar{1}1]$ differs according to the steel considered. The fiber texture <111>//ND is almost perfect in steels C and B although the levels are different, in contrast to what is observed in steel A in which the texture $(\bar{1}11)[0\bar{1}1]$ is predominant. Moreover, the deviation of the fiber texture towards $(5\bar{5}4)[2\bar{2}5]$ is observed more particularly in steels B and C. Strong deviations with respect to $(\bar{1}11)[\bar{1}\bar{1}0]$ are also observed in the same steels in which the predominant orientation would be $(\bar{2}23)[\bar{1}\bar{1}0]$; in steel A, the texture appears to be more ideally $(\bar{1}11)[\bar{1}\bar{1}0]$.

Strong elements of the partial fiber <110>//RD are superposed on the partial fiber texture <111>//ND. The former is particularly important in the case of steel B in which all the components between $(\bar{3}32)[\bar{1}\bar{1}0]$ and $(001)[\bar{1}\bar{1}0]$ are equally represented. The components are more differentiated in steel A, which has a major component $(\bar{1}11)[\bar{1}\bar{1}0]$ and a minor component $(\bar{1}13)[\bar{1}\bar{1}0]$. Steel C has $(\bar{2}23)[\bar{1}\bar{1}0]$ as the principal component, and the orientations ranging from $(\bar{1}12)[\bar{1}\bar{1}0]$ to $(001)[\bar{1}\bar{1}0]$ as the minor components.

TABLE II

CHARACTERIZATION OF SAMPLES FOR TEXTURE ANALYSIS

| Steel A | | | Steel B | | | Steel C | | |
|---|---|---|---|---|---|---|---|---|
| Reference | $\lvert\varepsilon_3\rvert_p$ | $\sigma_1 \equiv \sigma_2$ (MN $m^{-2}$) | Reference | $\lvert\varepsilon_3\rvert_p$ | $\sigma_1 \equiv \sigma_2$ (MN $m^{-2}$) | Reference | $\lvert\varepsilon_3\rvert_p$ | $\sigma_1 \equiv \sigma_2$ (MN $m^{-2}$) |
| AO | | 0 | BO | 0 | 0 | CO | 0 | 0 |
| AA | 0.098 | 380 | BA | 0.040 | 450 | CA | 0.032 | 340 |
| AB | 0.190 | 430 | BB | 0.154 | 570 | CB | 0.056 | 380 |
| AC | 0.280 | 475 | BC | 0.348 | 655 | CC | 0.090 | 415 |
| AD | 0.356 | 510 | BD | 0.382 | 665 | CD | 0.172 | 470 |
| AE | 0.408 | 540 | BE | 0.486 | 695 | CE | 0.304 | 515 |

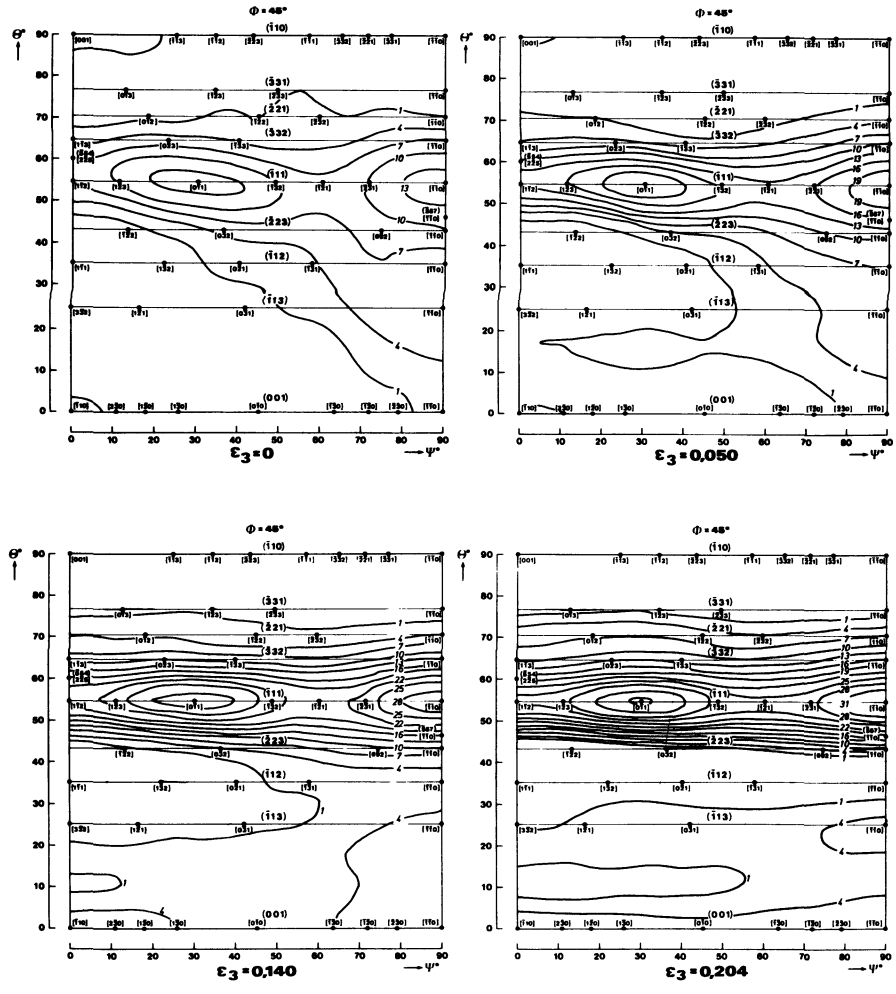


Fig. 2. Distribution function, $\phi$ = 45° section, A steel.

The intensity level of the components (001) is lower when the coefficient $\bar{r}$ is higher. In fact, the coefficients $\bar{r}$ of the steels are graded in the order of the ratios (111)/(100). It is, therefore, to be noted that the same coefficient of plastic anisotropy $\bar{r}$ can be obtained from quite different textures. Moreover, components ($\bar{1}$10)[uvw] are not observed in the three steels.

## 2.4. Deformation Textures

The crystalline texture changes as the deformation by biaxial expansion increases (Figs. 2 to 4). These textural changes are different in detail for the three steels but always lead to the strengthening of the textures <111>//ND and <100>//ND, which are the classical compression textures.[6-8] Thus the resulting textures in biaxial expansion are clearly different from those observed in uniaxial tension tests.[7,8]

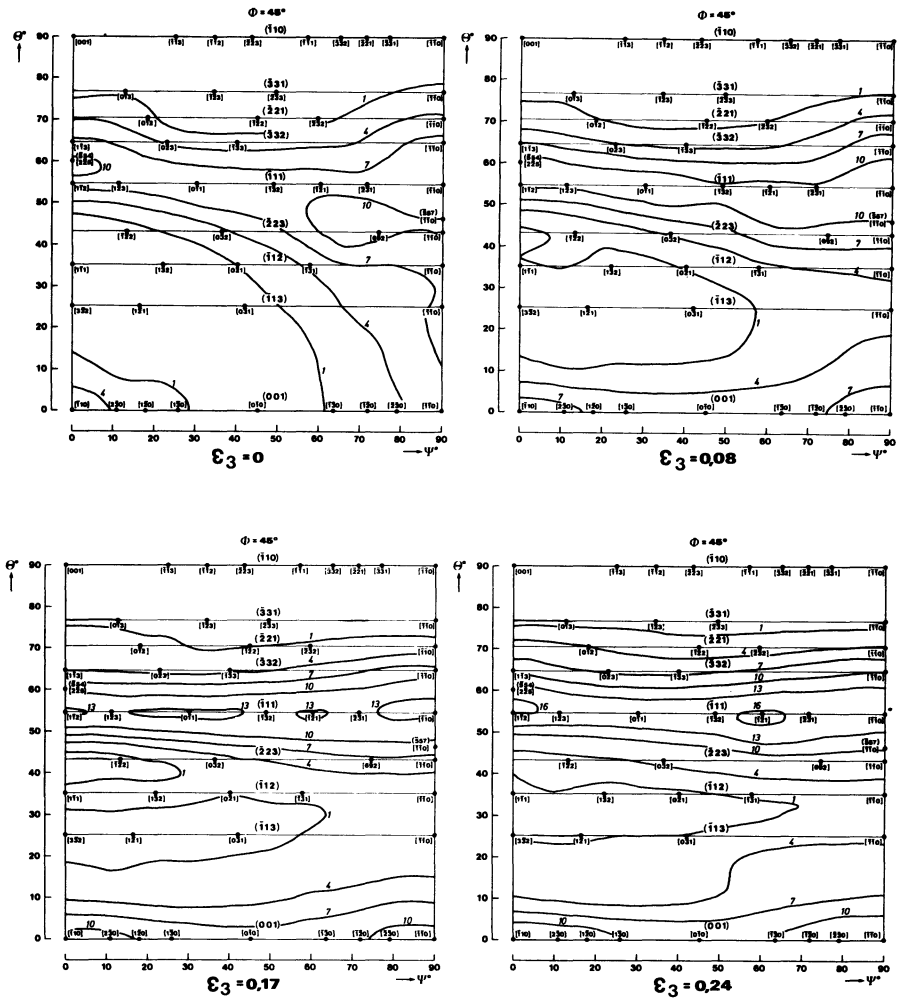


Fig. 3. Distribution function, $\phi = 45°$ section, B steel.

The evolution of the texture elements during deformation is not continuous; and it is possible for the three steels to show three successive stages in their development (Fig. 5). The first is represented by an increase of the fiber texture as a whole, that is to say of the components $(\bar{1}11)[0\bar{1}1]$ and $(\bar{1}11)[1\bar{1}2]$. Starting from a level of deformation close to $\varepsilon_{1.2} \simeq 0.10$, these textures become stable, and then increase again when necking is approached.

The textural modifications that are observed depend on the initial texture and on the characteristics inherent in the steel. Thus, the increase is very slight in steel B of which the initial texture is not very sharp. In the two other steels, A and C, the increases are significant. The two components $(\bar{1}11)[0\bar{1}1]$ and $(\bar{1}11)[1\bar{1}2]$ behave similarly in steel A, and somewhat differently in steel C, of which the initial texture is more ideally a fiber texture.

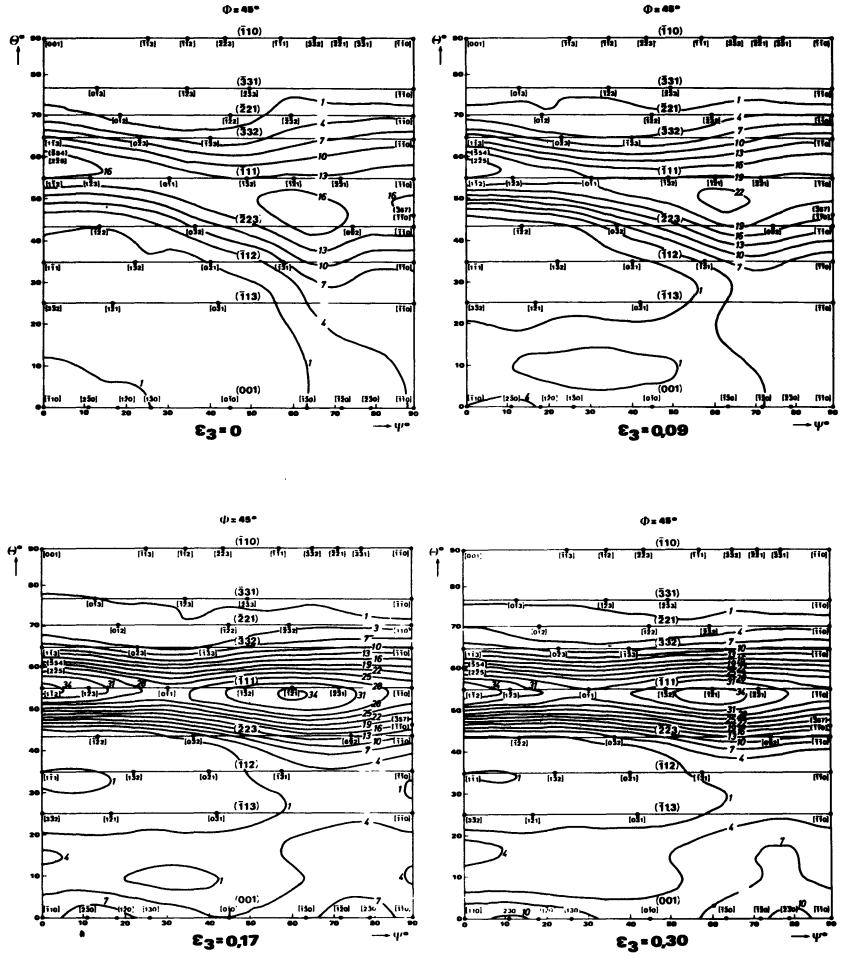


Fig. 4. Distribution function, $\phi = 45°$ section, C steel.

To this it must be added that in all cases the textures develop during expansion by becoming more and more ideal, and finally coinciding with the pure orientations at high strains.

The development of the components (100)[uvw] during deformation is substantially the same for the three steels (Fig. 6) so that the deformation textures <100>//ND depend essentially on their initial value and increase in the order A-C-B. As for the fiber texture <111>//ND, the actual development can be resolved into three phases for steels A and C.

Minor components also appear during equibiaxial expansion; this applies, for instance, to the orientations (113-114)[uvw] or (102-203)[uvw] which are well known to be associated with compression.[6] Also, minor components, more particularly (112)[uvw], which are present at the beginning of the deformation, undergo hardly any modifications even at high strains.

Thus the greatest textural modifications affect the fiber textures <111> and <001>//ND; the increase in <111>//ND in a

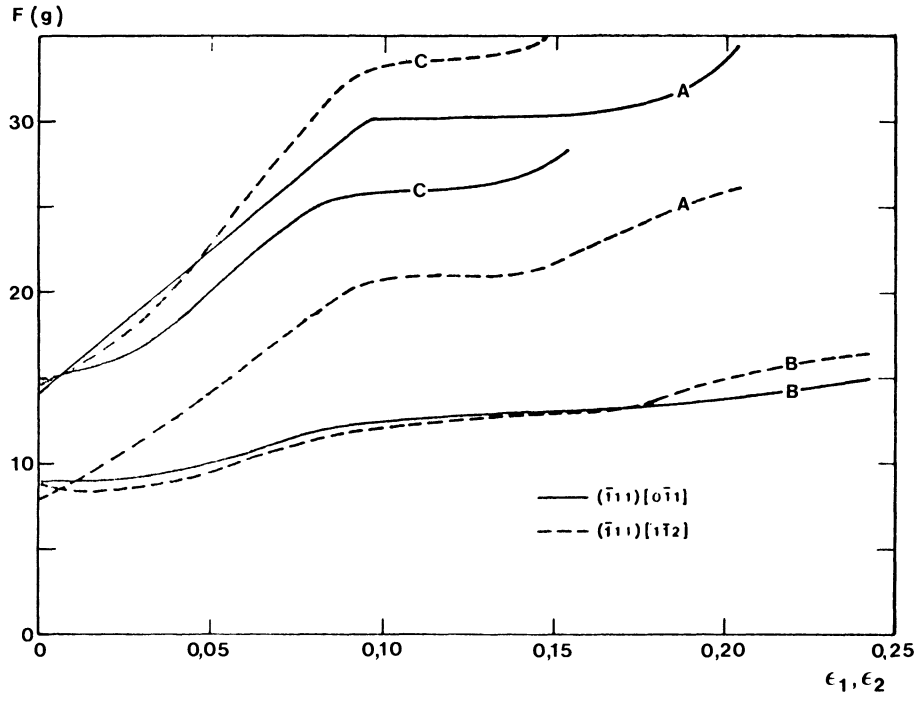


Fig. 5. Evolution of the <111> fiber texture in expansion.

high drawability steel takes place from the beginning of the deformation, whereas <001>//ND remains at a low level at first and only increases when a given deformation ($\varepsilon_{1,2} \gtrsim 0.05$, steel C; $\varepsilon_{1,2} \gtrsim 0.10$, steel A) has been reached. The increase in <111>//ND is not only less rapid in a steel of lower drawability (steel B) but also smaller; the reverse of this is true in the case of the texture <001>//ND. It is thus observed that in the case of a high-drawability steel the (111)/(100) ratio increases at the beginning of deformation, being opposite to what happens in a steel of lower drawability. Moreover, irrespective of the level of deformation rached, this ratio will be distinctly higher in the high-drawability steel than in the low-drawability steel.

## 3. DEVELOPMENT OF CRYSTALLINE TEXTURE IN MAXIMUM SHEAR PLANES

### 3.1. <111> Slip Directions Representation

The classical representation of texture in the referential RD, TD, ND does not make it possible to visualize the slip systems in maximum shear planes located at 45° from the axes of stresses. For this reason the function $[111]_{ij}F(\psi,\alpha)$ has been used in order to determine the distribution of the <111> slip directions in the macroscopic planes 13 and 23, in which the shear stresses are maximum during equibiaxial expansion (Fig. 7).

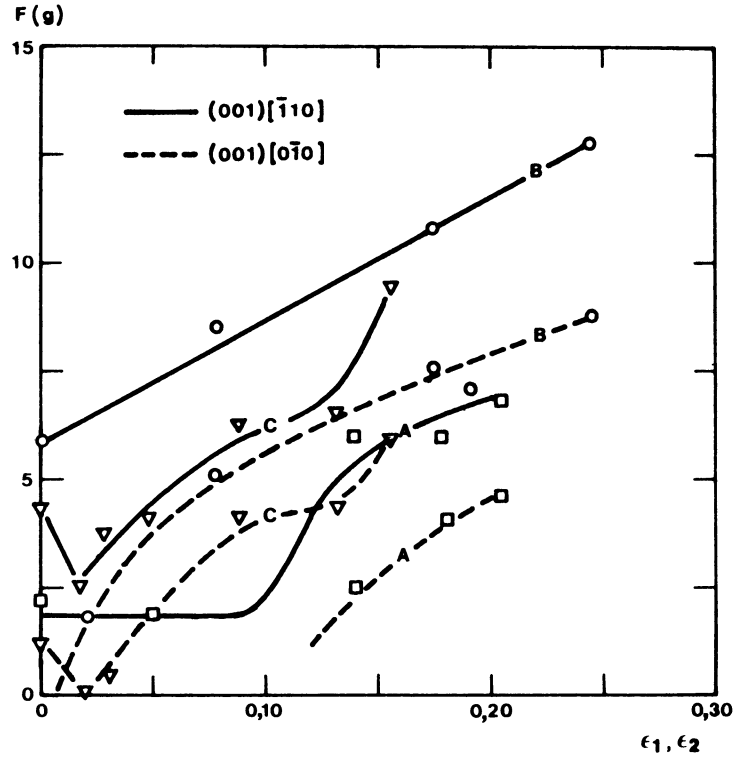


Fig. 6. Evolution of the <001> fiber texture in expansion.

The general expression[5] of this function is:

$$[111]_{ij}F(\psi,\alpha) = \sum_{\ell} \sum_{m} \sum_{n} D^{\ell}_{mn}\, Y^{mn}_{\ell}(o,\alpha,\psi) \qquad (1)$$

with

$$D^{\ell}_{mn} = \frac{1}{[Y^{mn}_{\ell}(o)]^2} \sum_{\mu} \sum_{s} f^{\ell}_{\mu s}\, Y^{\mu m}_{\ell}(g_{or}) \cdot Y^{ns}_{\ell}(90°,55°,45°)$$

where $\alpha \in [0,\frac{\pi}{2}]$ is the angle between the direction [111] considered and a reference direction $\vec{R}_o$ in the ij section.

The coefficients $f^{\ell}_{\mu s}$ are obtained from the experimental determination of the two pole figures {200} and {211} in the rolling plane[2,4]; the Euler angles of the rotation $g_{or}$ defining the shear plane considered are

plane 23: $g_{or}$ = (0,90,45) $\vec{R}_o$//RD

plane 13: $g_{or}$ = (90,90,135) $\vec{R}_o$//TD.

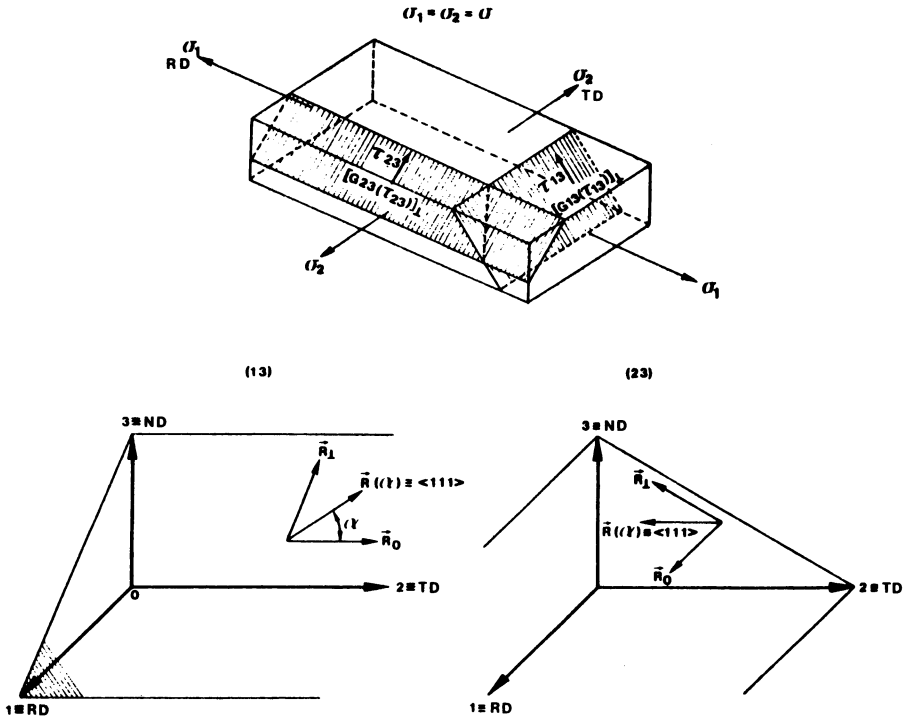


Fig. 7. Definition of the $\vec{R}(\alpha)$ direction in maximum shear planes (equibiaxial expansion).

Owing to the symmetry conditions in the material, the function ${}^{<111>}_{ij}F(\psi,\alpha)$ is calculated by means of the relationship (1), considering only the real parts $D^{\ell R}_{mn}$ of the complex coefficients $D^{\ell}_{mn}$, with $\ell$,m even and n = 4k.

### 3.2. <111> Directions Distribution Before Deformation

Before deformation the slip directions <111> are distributed differently in the macroscopic planes 13 and 23 (Fig. 8). In 13, the directions <111> are located in an angular region $\alpha \leq 50°$ defined from a reference direction $\vec{R}_o$ parallel to TD and their distribution is the most important in the interval $20° \lesssim \alpha \lesssim 25°$. These directions are associated in every case with crystallographic planes located half way between {123} and {110}.

The directions <111> in the plane 23 are contained within the region $\alpha\varepsilon[20°,50°]$ with a maximum density corresponding to $\alpha = 35°$; they are in this case associated with crystallographic slip planes {110}. Irrespective of the macroscopic plane, no slip system <111>{112} appears to be present; it is thus found that in these macroscopic planes 13 and 23 only the <111>{110} or adjacent slip systems will contribute to the deformation.

The density of the slip systems <111>{hk$\ell$} depends both on the steel and on the macroscopic plane considered. The

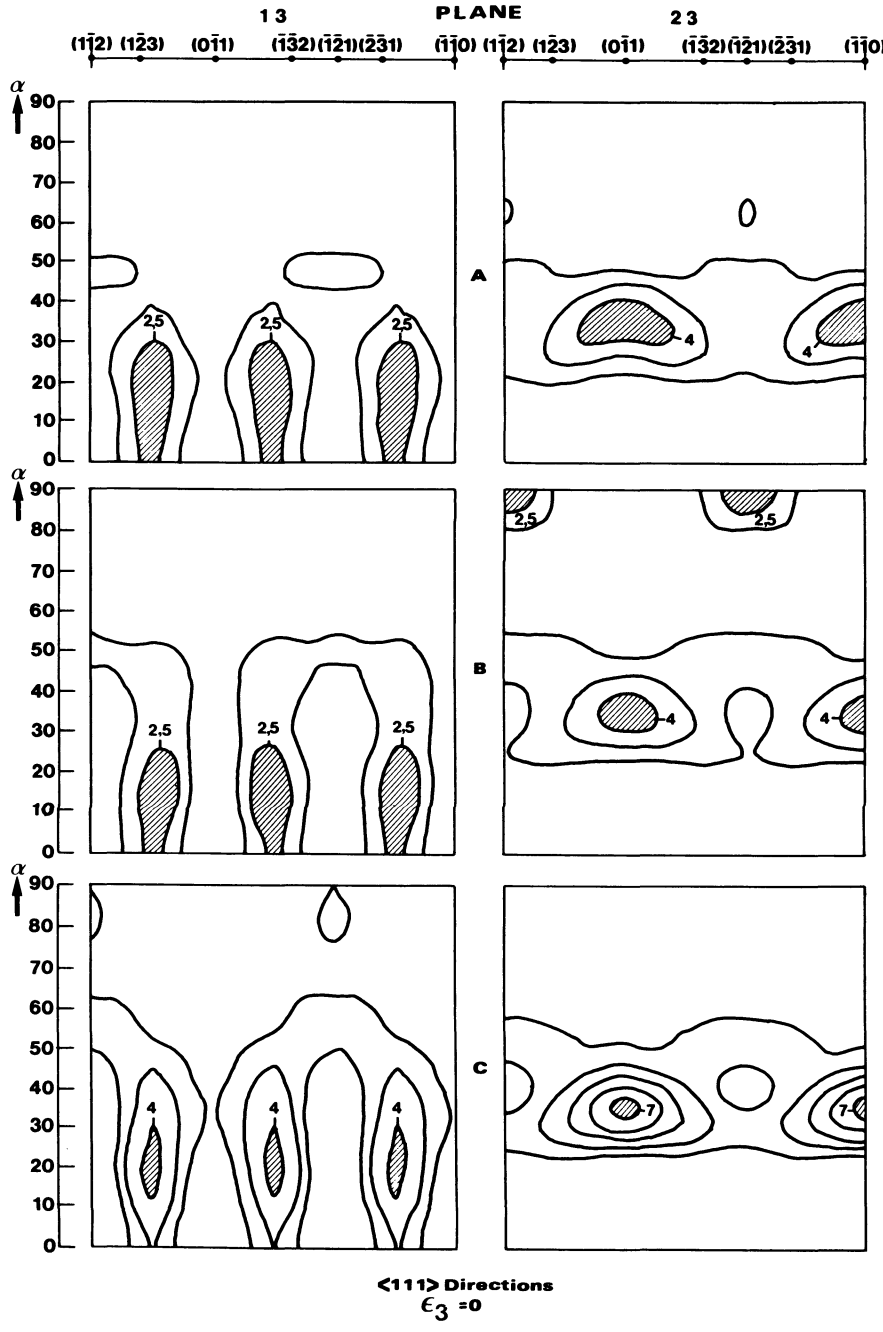


Fig. 8. Distribution of the slip systems in shear planes 13 and 23 before expansion.

steels may be classified according to this density, and this classification is the same for planes 13 and 23; the ease of gliding increases in the order B, A, C.

As shown by Fig. 7, the thinning of the steel depends essentially on the angle $\alpha$ between the direction $\vec{R}_o$ and the slip directions <111>. For the same applied stresses, the slip systems located at $\alpha$-angles lower than 45° will lead to less thinning than the slip systems with $\alpha$-angles higher than 45°.

The angular distribution $\alpha$ of the slip directions <111> must cause the resistance of the steels to thinning to increase in the order B, A, C, as it is confirmed by measurements of polar deformation $|\varepsilon_3|_p$ (Fig. 1). Moreover, as shown in Fig. 8, only steel B characterized by a low coefficient $\bar{r}$ has slip systems <111>{112} located at 90° from $\vec{R}_o$, that is to say capable of promoting the thinning of the material from the beginning of deformation.

### 3.3. <111> Directions Modifications During Expansion

Equibiaxial expansion modifies the configuration of the slip systems <111> in the shear planes 13 and 23 (Fig. 9).

The modifications of texture depend on the initial texture of the steel sheet and on the applied stresses. They appear from the beginning of deformation, although large rotations are in fact observed only at high levels of strain.

The modifications of texture are specific to the macroscopic shear plane examined. During the expansion the configurations of the slip systems <111> develop so as to become equivalent in the two maximum shear planes 13 and 23. This is in good agreement with the approach to the process of deformation that has been adopted, and, in particular, its description in the maximum shear planes, because in this model the stresses $\tau_{13}$ and $\tau_{23}$ in the planes 13 and 23 are equal during equibiaxial expansion.

Although the hypothesis of the pencil glide seems to be the best adapted to the description of the process of deformation, the different slip planes {hkℓ} associated with the directions <111> do not develop in the same way during deformation. The slip systems <111>{112}, which are initially of low density, decrease during expansion, being opposite to the systems <111>{110} - <111>{123} of which the densities increase.

In the shear plane 23 the principal orientation <111> {011} $\alpha$ = 35° which is present in the non-deformed state is dissociated during expansion into two components $\psi$ = 20°, $\alpha$ = 30° and $\psi$ = 30°, $\alpha$ = 45-50°. The first of these two components is more important in steels C and A of which the resistance to thinning is high. Moreover, the greater ease of thinning of the steel B is explained by strengthening of the slip orientation $\alpha$ = 45-50°.

As in the case of the shear plane 23, the modifications of the slip systems in the plane 13 lead to more thinning in the steel B. It is in the latter, in fact, that the most unfavorably oriented components of gliding ($\alpha$ = 55°) appear during deformation. These (Fig. 9) are very important, and, as will be noted, the rotation of the crystallites has progressed in such a way that the gliding occurs in the plane {110}. Although these rotations occur in steels A and C, they are limited so that the gliding remains mainly located in the

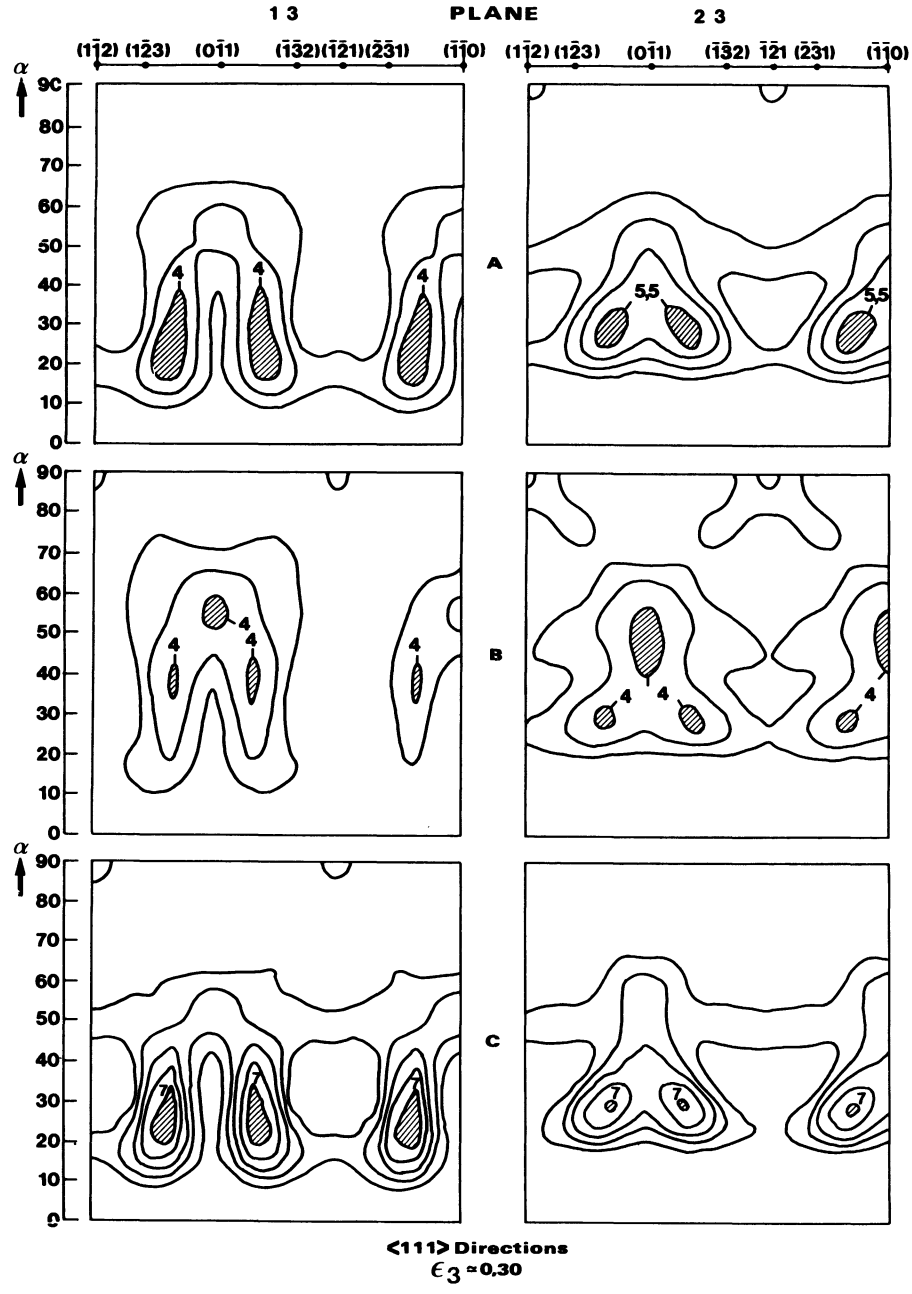


Fig. 9. Distribution of the slip systems in shear planes 13 and 23 after equibiaxial expansion ($|\varepsilon_3|_p \sim 0.30$).

planes {123} and leads, because of its localization ($\alpha$ = 25-30°), to less thinning. In regard to the resistance to thinning, the steels are thus graded in the order C, A, B when the plane 13 is considered.

# 4. PLASTIC DEFORMATION AND CRYSTALLINE TEXTURE

## 4.1. Mathematical Model

The deformation model proposed by D'Haeyer and Gouzou[1] supposes that all plastic deformation results from a superposition of plastic flow in the planes of the material in which the tangential stress is maximum, that is to say, the planes ij located at 45° from the principal stresses. In these planes ij the maximum tangential stress is expressed by $\tau_{ij} = \sigma_i - \sigma_j$ and is parallel to the direction $\vec{R}_\perp$.

The plastic flow in the planes ij are connected with displacements of dislocations which in the case of b.c.c. materials take place in the direction <111> (pencil glide).

As we have seen above, each plane ij of the material has an angular distribution ${}^{<111>}_{ij}F(\psi,\alpha)$ of crystallographic directions <111> associated with planes (hkℓ), this angular distribution being modified according to the plane (ij) during deformation.

Taking the hypothesis of the pencil glide, it is possible to define in the plane ij a density of crystallographic directions <111> in the direction $\vec{R}(\alpha)$ by the relationship:

$$D_{ij}(\alpha,\tau_{ij}) = \int_0^{2\pi} {}^{<111>}_{ij}F(\psi,\alpha,\tau_{ij})\, d\psi \qquad (2)$$

Let us consider the gliding $g_{ij}(\alpha,\tau_{ij})$ in the plane ij according to the direction $\vec{R}(\alpha)$ (Fig. 10); this gliding depends on the maximum shear stress $\tau_{ij}$ and on the density of the directions <111> in $\vec{R}(\alpha)$ by the relationship:

$$g_{ij}(\alpha,\tau_{ij}) = D_{ij}(\alpha,\tau_{ij})\ \gamma(\tau^{\alpha}_{ij}) \qquad (3)$$

where $\gamma(\tau_{ij})$ defines the elementary dislocations gliding corresponding to an orientation {hkℓ}<111> parallel to $\vec{R}(\alpha)$; $\tau^{\alpha}_{ij}$ is the component of the shear stress in $\vec{R}(\alpha)$ equal to $\tau^{\alpha}_{ij} = \tau_{ij} \sin\alpha$.

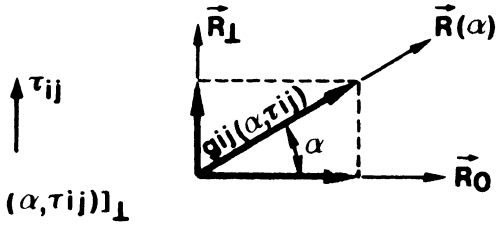


Fig. 10. Gliding in shear plane ij.

With the assumption that the hardening of the material during deformation arises essentially from dislocations-dislocations interactions in one and the same direction $\vec{R}(\alpha)$ and is therefore independent of the angle α, the elementary

gliding $\gamma(\tau_{ij}^{\alpha})$ depends only on the stress $\tau_{ij}^{\alpha}$:

$$\gamma(\tau_{ij}) = K(\tau_{ij}^{\alpha} - \tau_o)^{1/n_o} = K(\tau_{ij} \sin \alpha - \tau_o)^{1/n_o} \quad (4)$$

Taking into account the relationships (3) and (4), the gliding $g_{ij}(\alpha,\tau_{ij})$ in the direction $\vec{R}(\alpha)$ will be expressed in the form:

$$g_{ij}(\alpha,\tau_{ij}) = K\, D_{ij}(\alpha,\tau_{ij}) \times (\tau_{ij} \sin \alpha - \tau_o)^{1/n_o} \quad (5)$$

The contribution of this gliding in the direction of the shear stress $\tau_{ij}$ (direction $\vec{R}_{\perp}$) will be equal to:

$$[g_{ij}(\alpha,\tau_{ij})]_{\perp} = g_{ij}(\alpha,\tau_{ij}) \sin \alpha \quad (6)$$

Now, the resultant macroscopic gliding in the direction of the tangential stress $\tau_{ij}$ (direction $\vec{R}_{\perp}$) will be obtained by angular integration of the elementary glidings in the plane ij:

$$[G_{ij}(\tau_{ij})]_{\perp} = \int_0^{\pi} [g_{ij}(\alpha,\tau_{ij})]_{\perp}\, d\alpha \quad (7)$$

These macroscopic glidings in the direction $\vec{R}_{\perp}$ lead to the deformations $\varepsilon_{i,j,k}$ in the principal directions i,j,k (RD, TD and ND for thin sheets) by use of the relationship

$$\varepsilon_{ij} = [G_{ij}(\tau_{ij})] - [G_{ki}(\tau_{ki})] \quad i,j,k \quad (8)$$

## 4.2. Application to Equibiaxial Expansion

In equibiaxial expansion, the principal stresses $\sigma_1$(// to RD) and $\sigma_2$(// to TD) are equal and the stress $\sigma_3$(// to ND) is zero. The tangential stresses are then maximum in the planes 13 and 23 at 45 degrees from the normal and transverse directions on the one hand and the normal and rolling directions on the other, and are expressed by

$$\tau_{13} = \tau_{23} = \sigma/2 = \tau \text{ with } \sigma_1 = \sigma_2 = \sigma$$

$$\tau_{12} = 0$$

In this case, the principal deformations $\varepsilon_1^E$, $\varepsilon_2^E$, $\varepsilon_3^E$ are connected with the macroscopic glidings $[G_{ij}(\tau_{ij})]_{\perp}$ in the maximum shear planes 13 and 23 by the relationships:

$$\varepsilon_1^E(\sigma) = G_{13}(\tau)$$

$$\varepsilon_2^E(\sigma) = G_{23}(\tau)$$

$$\varepsilon_3^E(\sigma) = -[G_{13}(\tau) + G_{23}(\tau)] \quad (9)$$

or more explicitly, taking into account the relationships shown above, by:

$$\varepsilon_1^E(\sigma) = K \int_o^{\pi} D_{13}(\alpha,\tau) \times (\tau \sin \alpha - \tau_o)^{1/n_o} \sin \alpha d\alpha$$

$$\varepsilon_2^E(\sigma) = K \int_o^{\pi} D_{23}(\alpha,\tau) \times (\tau \sin \alpha - \tau_o)^{1/n_o} \sin \alpha d\alpha \qquad (10)$$

$$\varepsilon_3^E(\sigma) = -K \int_o^{\pi} [D_{13}(\alpha,\tau) + D_{23}(\alpha,\tau)] \times (\tau \sin \alpha - \tau_o)^{1/n_o} \sin \alpha d\alpha$$

with $\sigma = \sigma_1 = \sigma_2$; $\tau = \tau_{13} = \tau_{23} = \sigma/2$.

The measurement of the variation in thickness of the sheet at the top of the drawn pieces as a function of the stress $\sigma = \sigma_1 = \sigma_2$ during expansion makes it possible, if the variation of the distribution function ${}^{<111>}_{ij}F(\psi,\alpha,\tau_{ij})$ is taken into account, to determine by a least square method the coefficients K, $n_o$, $\tau_o$ which appear in the relationships (10)[9] (Table III).

TABLE III

COEFFICIENTS OF STRAIN HARDENING LAW

| Steel | $\tau_o$ (MN $m^{-2}$) | K | $1/n_o$ | $n_o$ |
|---|---|---|---|---|
| A | 60 | $2.77\ 10^{-3}$ | 1.25 | 0.80 |
| B | 90 | $2.98\ 10^{-7}$ | 2.90 | 0.34 |
| C | 45 | $1.12\ 10^{-6}$ | 2.70 | 0.37 |

The critical stress $\tau_o$ corresponds to the threshold of microplastic deformation in a uniaxial tensile test.

Thus defined, the strain hardening rate $n_o$ is independent of the crystalline texture of the material, which is not so in the case of the strain hardening rate in uniaxial deformation $\bar{n}$ and in symmetrical biaxial expansion n*. This strain hardening rate $n_o$ is particularly high for steel A of which the grain size is large (26 μ).

When the values of coefficients K, $n_o$, $\tau_o$ are taken into account the deformations $|\varepsilon|_3$ calculated by means of the relationships (10) agree very well with the experimental curves of deformations of the three steels studied (Fig. 11).

## 4.3. Stretchability of the Steels

The analytical model developed above makes it possible to define a coefficient of equibiaxiality of deformations $\Delta = \varepsilon_1/\varepsilon_2$. This coefficient, calculated by means of the relationships (10), depends on the initial angular distribution of the directions <111> in the shear planes 23 and

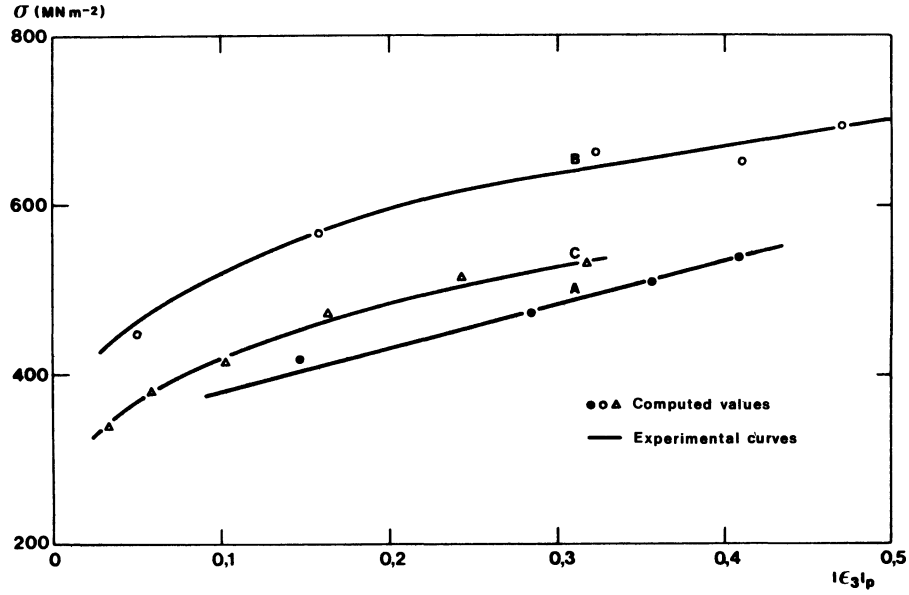


Fig. 11. Stress-strain relationships in equibiaxial expansion.

13 and on their modifications during expansion. It in fact represents the steel ability to distribute its principal deformations isotropically during expansion.

TABLE IV

EQUIBIAXIALITY COEFFICIENTS Δ OF STEELS

| Steel A | | Steel B | | Steel C | |
|---|---|---|---|---|---|
| τ | Δ | τ | Δ | τ | Δ |
| 190 | 0.72 | 225 | 0.48 | 170 | 1.19 |
| 215 | 0.68 | 285 | 0.75 | 190 | 0.98 |
| 237 | 0.77 | 328 | 0.85 | 208 | 0.91 |
| 255 | 0.85 | 333 | 0.77 | 236 | 1.11 |
| 270 | 0.81 | 348 | 0.76 | 258 | 1.10 |

Table IV shows the coefficients Δ of the three steels, calculated for different levels of applied stress σ. For steel C, the coefficient Δ is close to unity, and therefore equibiaxiality of the principal strains $\sigma_1$ and $\sigma_2$ is practically obtained; for steels A and B, the strain $\sigma_2$ is higher than the strain $\sigma_1$ irrespective of the level of applied stress.

This analysis enables the understanding of the various behaviors of the steels during expansion with the aid of three essential parameters: the angular distribution $\vec{R}(\alpha)$ of the slip directions <111> in the maximum shear planes, the coefficient of equibiaxiality $\Delta$ and the strain hardening rate $n_o$.

For steel C the particular distribution of the <111> slip directions in the shear planes 13 and 23 is such that equibiaxiality of the deformations $\varepsilon_1$ and $\varepsilon_2$ ($\Delta \simeq 1$) is almost obtained together with a good resistance to thinning (the distribution $\vec{R}(\alpha)$ is located at the angles $\alpha < 45°$); steel C is therefore particularly suitable for equibiaxial expansion in spite of its low hardening strain rate $n_o$.

Owing to its worse equibiaxiality coefficient ($\Delta < 1$) and the presence of slip systems promoting thinning (distribution $\vec{R}(\alpha)$ for angles $\alpha > 45°$), steel B has a less favorable behavior during expansion. In regard to steel A, the low equibiaxiality coefficient ($\Delta < 1$), balanced by a good distribution of the slip systems $\vec{R}(\alpha)$ and above all by a high strain hardening rate ($n_o = 0.8$) accounts for the medium behavior of this steel during expansion.

## CONCLUSIONS

Textural modifications during equibiaxial expansion are towards the classical compression configurations <111> and <100>//ND; minor components (114)[uvw] and (102)[uvw] also appear in accordance with the theory. The magnitude of the modifications observed depends both on the deformation ($\varepsilon$) and on the initial texture of the steel: a high drawability steel is characterized by a large (111)/(100) ratio which increases during expansion.

The three-dimensional analysis does not make it possible to understand the mechanisms of the deformation and, in particular, to separate the true hardening of the material from the textural effects (rotations). The generalization of this analysis in the maximum shear planes has enabled us to analyze and quantify the configuration of the slip systems. This allows the development of a deformation model which takes into account the factors influencing the degree of stretchability of the steels.

From this model it is possible to define true hardening rates very different from those determined by mechanical tests, and equibiaxiality coefficients characterizing the ability of the steel to distribute the deformation in the macroscopic shear planes. These two parameters in association with the resistance to thinning defined by the configuration of the slip systems in the macroscopic shear planes make it possible to grade the different steels in such a manner that the theoretical behavior calculated on the basis of these parameters is very close to the experimental results.

## ACKNOWLEDGEMENTS

The authors would like to thank all the people at the C.R.M. who contributed to this investigation and especially Mrs. J. Gouzou, L. Habraken and R. D'Haeyer for fruitful

discussions. This research has been carried out with financial support of IRSIA (Institut pour l'encouragement de la Recherche Scientifique dans l'Industrie et l'Agriculture) and CECA (Communautés Européennes du Charbon et de l'Acier).

REFERENCES

1. R. D'Haeyer and J. Gouzou, *C. R. Acad. Sc. Paris*, 280, B-737 (1975).
2. R. J. Roe, *J. Appl. Phys.*, 36, 2024 (1965).
3. H. J. Bunge, *Mathematical Methods of Texture Analysis*. (Akademie-Verlag, Berlin, 1969).
4. C. Gaspard, P. Messien and J. Mignon, C.R.M. Internal Report MP 13/76 (1976).
5. C. Gaspard, P. Messien and J. Mignon, "Method for orientations distribution function analysis in maximum shear planes," in *Proc.5th Int. Conf. on Texture of Matls.* (ICOTOM-5), Aachen, March 1978 (in press).
6. A. Calnan and C. J. B. Clews, *Phil. Mag.*, 42, 616 (1951).
7. P. Messien, A. de Leval and J. Jacob, in *Proc. 3rd European Congr. on Textures*, Pont-à-Mousson, p. 629, June 1973.
8. B. Baudelet et al., "Drawing limit curves - Microstructural analysis of the effect of deformation paths," to be published in *Mem. Sc. Rev. Met.*
9. P. Messien, C. Gaspard, J. Mignon and T. Greday, "Texture hardening in maximum shear planes during expansion," in *Proc. 5th Int. Conf. on Texture of Matls.* (ICOTOM-5), Aachen, March 1978 (in press).